AGU PUBLICATIONS

JGR

Journal of Geophysical Research: Space Physics

RESEARCH ARTICLE
10.1002/2017JA024023

Key Points:
- Strong day and nighttime VLF signal anomalies associated with December 2012 TC Evan
- The maximum increase in the daytime *D* region VLF reference height by 7.5 km
- Morlet wavelet analysis of VLF signal amplitude gives strong wave-like signatures associated with this TC

Correspondence to:
S. Kumar,
kumar_su@usp.ac.fj

Citation:
Kumar, S., S. NaitAmor, O. Chanrion, and T. Neubert (2017), Perturbations to the lower ionosphere by tropical cyclone Evan in the South Pacific Region, *J. Geophys. Res. Space Physics*, *122*, doi:10.1002/2017JA024023.

Received 11 FEB 2017
Accepted 20 JUN 2017
Accepted article online 22 JUN 2017

Perturbations to the lower ionosphere by tropical cyclone Evan in the South Pacific Region

Sushil Kumar[1], Samir NaitAmor[2], Olivier Chanrion[3], and Torsten Neubert[3]

[1]School of Engineering and Physics, University of the South Pacific, Suva, Fiji, [2]Astrophysics Division, CRAAG, Algiers, Algeria, [3]National Space Institute, Technical University of Denmark, Lyngby, Denmark

Abstract Very low frequency (VLF) electromagnetic signals from navigational transmitters propagate worldwide in the Earth-ionosphere waveguide formed by the Earth and the electrically conducting lower ionosphere. Changes in the signal properties are signatures of variations in the conductivity of the reflecting boundary of the lower ionosphere which is located in the mesosphere and lower thermosphere, and their analysis is, therefore, a way to study processes in these remote regions. Here we present a study on amplitude perturbations of local origin on the VLF transmitter signals (NPM, NLK, NAA, and JJI) observed during tropical cyclone (TC) Evan, 9–16 December 2012 when TC was in the proximity of the transmitter-receiver links. We observed a maximum amplitude perturbation of 5.7 dB on JJI transmitter during 16 December event. From Long Wave Propagation Capability model applied to three selected events we estimate a maximum decrease in the nighttime *D* region reference height (H') by ~5.2 km (13 December, NPM) and maximum increase in the daytime *D* region H' by 6.1 km and 7.5 km (14 and 16 December, JJI). The results suggest that the TC caused the neutral densities of the mesosphere and lower thermosphere to lift and sink (bringing the lower ionosphere with it), an effect that may be mediated by gravity waves generated by the TC. The perturbations were observed before the storm was classified as a TC, at a time when it was a tropical depression, suggesting the broader conclusion that severe convective storms, in general, perturb the mesosphere and the stratosphere through which the perturbations propagate.

1. Introduction

Signals from navigational transmitters are one of few tools available for remote sensing of the mesosphere-lower thermosphere region at 60–130 km altitude [*Silber and Price*, 2016]. Emitted at specific frequencies in the very low frequency band (VLF, 3–30 kHz), the signals propagate long distances in the Earth-ionosphere waveguide by multiple reflections at the electrically conducting boundaries of the Earth's surface and the lower ionosphere (*D* region) at 50–90 km [*Barr et al.*, 2000]. The *D* region is the lowest part of the Earth's ionosphere and is referred here to as daytime *D* region and nighttime *D* region [*Thomson and McRae*, 2009]. It can be viewed as a variable upper wall of the waveguide, and studies of its variations using the VLF technique have given insight into its physics. For example, the region is affected from above mainly by the Lyman α radiation from the Sun [*Thomson et al.*, 2014] and the diurnal and seasonal variations in the incoming solar flux and is sensitive to impulsive events on the Sun such as coronal mass ejections if these hit the magnetosphere and cause enhanced ionization from energetic particle precipitation and enhanced electric currents heating the upper mesosphere-lower thermosphere [*Beharrell et al.*, 2015]. From below, electromagnetic radiation from lightning may scatter energetic electrons of the magnetosphere into the atmosphere increasing its ionization [e.g., *Peter and Inan*, 2005] by energetic electron precipitation, and thunderstorms may directly affect the mesosphere through ionization and heating of the lower ionospheric plasma by transient luminous events (TLEs): sprites, elves, and gigantic jets [e.g., *Haldoupis et al.*, 2012] and by perturbations of the attachment rates of free electrons by the electromagnetic pulses from lightning [*Marshall et al.*, 2008]. In the present study we use the VLF technique to measure perturbations to the lower ionosphere properties and suggest that they are mediated by gravity waves (GWs), a source that does not directly modify ionization of the region but affects the motion of the background atmosphere that will carry the lower ionosphere with it and thereby modulate the reflection altitude of VLF waves.

The troposphere can generate atmospheric acoustic/gravity waves that deposit energy and momentum in the mesosphere and drive its interhemispherical circulation [e.g., *Garcia and Solomon*, 1985]. The sources considered are topographic (winds over mountains), deep convection (thunderstorms and cyclones) and wind shear (frontal weather systems and jet streams) [e.g., *Sato et al.*, 2009]. The GWs propagate obliquely

upward and couple to the ionosphere through ion-neutral collisions; their propagation properties can be altered by background wind [*Cowling et al.*, 1971]. Observational evidence for GWs in the stratosphere and mesosphere is primarily from satellites, soundings, and radars; however, for convective sources their characterization is lacking because of the intermittent nature of storms, the variety of convectively generated modes, and the large range of propagation angles that may extend their influence at horizontal distances far from the source [*Fritts and Alexander*, 2003].

The Pacific Ocean offers large expanses without topographic features and is therefore a region well suited to study the characteristics of convective sources. However, of these, thunderstorms normally occur over land, leaving tropical depressions, developing into hurricanes, and tropical cyclones (TCs), as the main source. Some recent experimental studies show that cyclones generate a wide spectrum of GWs in the lower stratosphere as detected in (MU) middle and upper atmosphere radar data [*Dhaka et al.*, 2003] and by combining data from GPS occultation and atmospheric sounding balloons with numerical weather models and simulations [*Ming et al.*, 2014], and a few studies suggest that disturbances may be induced in the *F* region of the ionosphere, observed in radar data [*Xiao et al.*, 2007] and GPS data [*Perevalova and Ishin*, 2011]. Recent studies include *Song et al.* [2017] that report medium-scale traveling ionospheric disturbances with period 40–57 min excited during landfall of typhoons Rammasum and Matmo, detected in the total electron content data from a GPS network in China, and *Vanina-Dart and Sharkov* [2016] who conclude that internal GWs associated with cyclones are the main source that affects the tropical ionosphere from below.

The VLF transmitter signal technique to probe the mesosphere has been shown to be sensitive to acoustic and GWs generated by the motion of the sunrise and sunset terminator for wavelengths $>$20 km [*Nina and Čadež*, 2013], which is comparable to the transmitter signal wavelengths, and the method was recently used to study a number of cyclones in the north-eastern Pacific region. It was found that six out of eight cyclones had nighttime anomalies in the signal amplitude during 1–2 days when the cyclones were inside the sensitivity zones of the transmitter signals [*Rozhnoi et al.*, 2014]. The conclusions reached in observational studies are corroborated by high-resolution simulations of GWs generated by typhoons reaching the lower thermosphere (100 km altitude) and extending thousands of kilometer from the storm center [*Liu et al.*, 2014].

In this work we complement the few studies conducted so far of cyclone perturbations to the mesosphere by analyzing anomalies in VLF transmitter signals recorded at Suva, Fiji, due to TC Evan during 9–23 December 2012, in proximity of Samoa and Fiji. We estimate the changes in the lower ionospheric Wait parameters (reference height and density gradient) using the Long-Wavelength Propagation Capability (LWPC) code [*Ferguson*, 1998] and characterize the TC associated waves by a Morlet wavelet analysis of the signals amplitude [*Mallat*, 1998].

2. Data and the Method of Analysis

A tropical depression was formed on 9 December about 700 km northeast of Fiji. On 12 December, it intensified to a category 2 TC named Evan and moved eastward and closer to Samoa where it was stationary for about 24 h. On 13 December, Evan moved slowly away from Upolu, Samoa, curved westward and intensified to category 4. It continued past the French Island Territories of Wallis and Futuna and reached Fiji, on 17 December. The following days it continued southwest and gradually lost strength [*World Meteorological Organization*, 2013]. Evan caused widespread destruction of infrastructure and loss of property, particularly in Samoa (Reliefweb, 2013, http://reliefweb.int/disaster/tc-2012-000201-wsm). The track and its strength are shown in Figure 1a.

Evan was unique in the sense that it recurved around Samoa and stayed for about 24 h over Samoa affecting the VLF transmitter signals recorded in Suva, Fiji, from two transmitters on mainland USA (NAA and NLK) and one on Hawaii (NPM). Moving toward and past Fiji, it intercepted signals from transmitters in Japan (JJI), India (VTX3), and Australia (NWC). The great circle paths of the transmitter-receiver links are shown in Figure 1b, and data on the transmitters and the maximum signal amplitude perturbations during the storm (see next section), and their transmitter-receiver great circle path (TRGCP) lengths are shown in Table 1.

The receiver is located at Suva (18.14°S, 178.44°E) and consists of a vertical electric field antenna and a SoftPAL (Software-based Phase and Amplitude Logger) that allows storing of narrowband data with 10–100 ms of resolution at several frequencies simultaneously. In our analysis we have used 1 min averaged data obtained from recording at 100 ms resolution. The quiet day, diurnal signal amplitude is determined from the

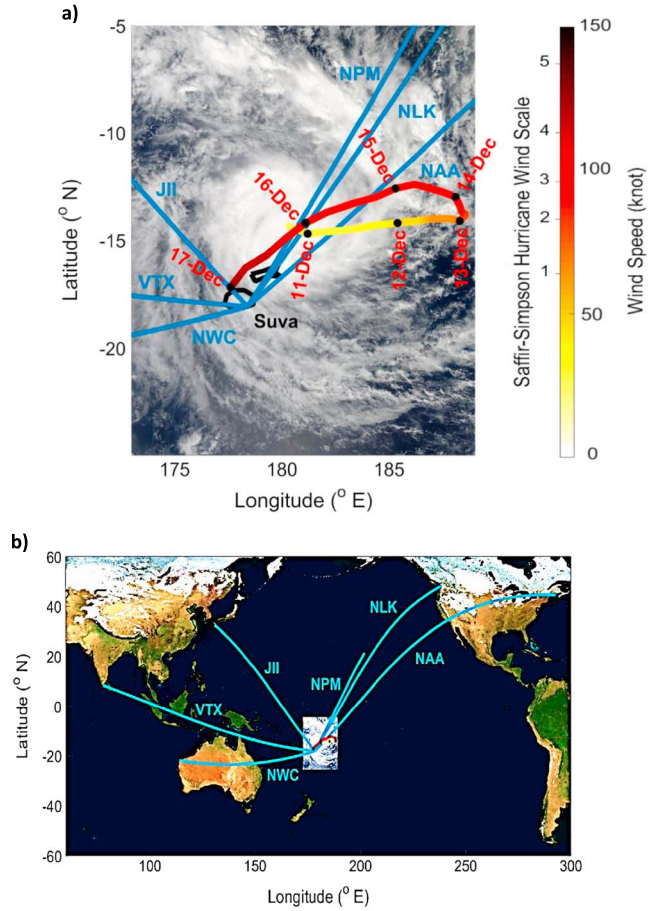

Figure 1. (a) The TC path and strength on different days during 11–17 December 2012. The path color shows the TC strength (wind speed). An image from the Moderate Resolution Imaging Spectroradiometer instrument of tropical cyclone Evan has been overlaid, (b) transmitter-receiver great circle paths (blue), the cyclone track (red), and VLF recording station Suva, Fiji (black).

8 normal days preceding the storm together with the standard deviation, and amplitudes during the storm phase exceeding 3 standard deviation (σ) are considered as strong anomalies caused by the cyclone. Since the cyclone started to form on 9 December, the normal days are 1 to 8 December and the disturbed days 9 to 16 December at 03:42 UT when power was cut in Suva as the storm hit Fiji.

In addition to the data analysis, the LWPC V2.1 signal propagation code is used to estimate the perturbations to the *D* region [*Ferguson*, 1998]. The code utilizes a modal solution, treating the Earth-ionosphere waveguide as a parallel-plate structure, with an imperfect ground, and an anisotropic magnetized collisional ionospheric plasma for the upper boundary. The curvature of the Earth is taken into account via a correction factor as a function of distance [*Ferguson and Snyder*, 1987]. A given transmitter-receiver path is divided into segments, and the wave electric field is sequentially calculated at each segment with the ground conductivity and permittivity taken into account from real data embedded into the code. It is assumed that the ionosphere is infinite, homogenous, and uniform in the horizontal dimension transverse to the propagating path [*Poulsen et al.*, 1993a] which during daytime is appropriate for shorter signal propagation path.

The code assumes a *D* region that is approximated with the Wait model of the lower ionosphere which is characterized by two parameters: the sharpness β and reference height H' [*Wait and Spies*, 1964]. In this model, the electron density N_e as a function of height h is given as follows:

$$N_e(h) = 1.43\times10^7 \mathrm{cm}^{-3}\left[\exp\left(-0.15H'\right)\exp\left[(\beta-0.15)\left(h-H'\right)\right]\right] \quad 50\leq h\leq 90, \tag{1}$$

where H' is in km and β in km^{-1}. This formulation is commonly used in research using the technique of VLF

Table 1. Data on the VLF Transmitters Recorded on Fiji Along With Their Transmitter-Receiver Great Circle Path (TRGCP) Distance

Transmitter	Frequency (kHz)	Location	Coordinates	TRGCP Distance (Mm)	Max Amplitude Anomaly (dB)
NAA	24.0	Cutler, Main, USA	44.65°N, 67.28°W	12.25	−6.9
NLK	24.8	Jim Creek, Washington, USA	48.20°N, 121.92°W	9.43	−3
NPM	21.4	Lualualei, Hawaii	21.42°N, 158.15°W	5.07	−4
JJI	22.2	Elbino, Japan	32.05°N, 130.83°E	7.50	−5.7
VTX3	18.2	Kanyakumari, India	8.39°N, 77.75°E	11.43	Off the air
NWC	19.8	North West Cape, Australia	21.82°S, 114.16°E	6.69	None

signals [e.g., *Thomson and McRae*, 2009; *Thomson et al.*, 2014]. With the geographic location of the transmitter and the receiver and the time in UTC as inputs, the code determines a single ambient value of each of the two parameters which is used for the complete transmitter-receiver link [*Poulsen et al.*, 1993a]. For daytime signal propagation, the influence of solar radiation on the *D* region parameters is applied assuming a constant solar zenith angle (SZA) along the path corresponding to the midpoint of the path [*McRae and Thomson*, 2000; *Thomson et al.*, 2014] with the relationship to H' and β given by *McRae and Thomson* [2000].

With this parametrization of the *D* region, the code has been shown to work well during the daytime [*McRae and Thomson*, 2000] but not so well at nighttime where the ionosphere is more disturbed for transequatorial passes because of scattering and mode conversion caused by the equatorial electrojet. The anomalous effects in the nighttime amplitude and/or phase of transequatorial signals have long been observed [*Lynn*, 1967, *Araki*, 1973; *Kikuchi*, 1983] and were explained by *Thomson and McRae* [2009]. However, this is a minor concern for our use of the code where we essentially explore the sensitivity of the signal amplitude to the localized perturbations; e.g., we are not interested in the quality of the fit between the code amplitude and the measured amplitude but in the magnitude of the perturbation to the amplitude. The perturbation to the undisturbed amplitude, determined as described above, is next found by introducing a localized perturbation in the segment in proximity to a disturbance. Here we assume that H' and β vary as a Gaussian and iterate to find the maximum of the Gaussian that gives the best fit to the perturbation magnitude of the signal parameters that are amplitude or amplitude and phase both.

We finally estimate the frequencies of the wave-like signatures (WLS) in the signals that may be associated with atmospheric GWs by applying the mother Morlet wavelet technique on the signals amplitude during the disturbed periods [*Mallat*, 1998; *Sauli et al.*, 2006]. The wavelet transform of the signal $x(t, z)$ is given as follows [*Sauli et al.*, 2006]:

$$T_x(a,u,z) = \frac{1}{\sqrt{a}}\int_{-\infty}^{+\infty} x(t,z)\ \Psi_0^*\left(\frac{t-u}{a}\right)\mathrm{d}t \tag{2}$$

where $T_x(a, u, z)$ is the wavelet transform of $x(t, z)$ which is the amplitude (z) and time (t) series, and Ψ_0 is the mother wavelet function. The a is positive and defines the scale of the analyzing wavelets, and u is a real number that defines the shift. For details on wavelet transforms, the reader is referred to *Mallat* [1998] and *Kumar and Georgiou* [1997].

3. Results

3.1. VLF Transmitters Signal Analysis

At low and middle latitudes, the diurnal variation of VLF signals is very stable in the daytime except during forcing of the ionosphere by solar flares and geomagnetic storms but is quite variable during the night [*Kumar et al.*, 2015]. The geomagnetic conditions during TC Evan were quiet with *Dst* index varying from +16 nT to −10 nT during 9–14 December and decreased to normal at −27 nT on 16 December at 13:00 UT (World Data Center, http://wdc.kugi.kyoto-u.ac.jp/).

As shown in Figure 1, the links to NAA, NLK, and NPM were intercepted by TC Evan twice as its track curved around Samoa, at the same time growing to category 4. Samoa is about 1150 km from Fiji in the northeastern direction. Heading toward Fiji, TC then passed the links to JJI, VTX3, and NWC in close proximity to the receiver. The VTX3 transmitter was off the air, and no anomalies were detected in the signal from NWC, likely because the TC was away from its sensitive zone until 03:42 LT on 16 December when the grid power in Fiji was turned off. Although the phase is also recorded, its use is rather complex because it drifts over the days and changes randomly when transmitters are turned on after maintenance. The following is then our analysis of the signals amplitude of the remaining four transmitters (NPM, NLK, NAA, and JJI) that all have transequatorial links to the Suva receiver.

The signal amplitudes are shown in Figure 2 for three periods of 24 h during the storm. The periods start at 04:00 UT on 10, 13, and 15 of December, thereby covering the last ~24 h before power was cut on 16 of December. The days correspond to different stages of the storm and its location; on the 3 days the storm was (1) a tropical depression close to the receiver, (2) category 3 and farthest from the transmitter links, and (3) category 4 closing in on the receiver. The red curves are the signal amplitudes, $A(t)$, the black curves are the mean amplitudes, $\hat{A}(t)$,and the gray curves are $\hat{A}(t)\pm 3\sigma(t)$, where σ is the standard deviation (rms

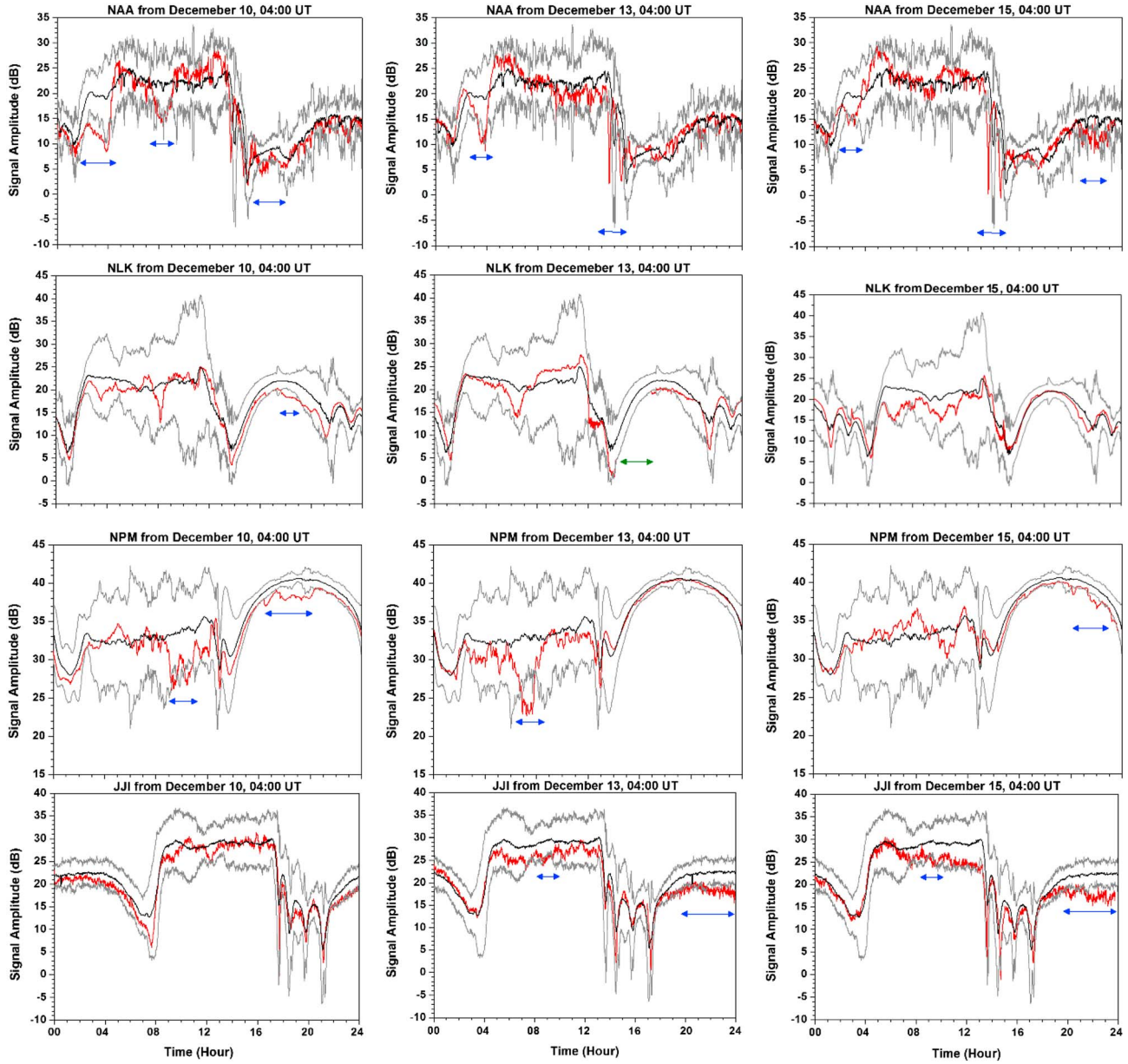

Figure 2. The signal amplitude, $A(t)$ (red) during 3 days (columns) for the four transmitters (rows) as function of time starting at 04:00 UT of each day for 24 h (00–24) as shown. The right column shows the last 24 h before the receiver lost power. Also shown are the quite mean amplitudes, $\hat{A}(t)$ (black), and $A(t) \pm 3\,\sigma(t)$ (grey). Amplitude excursions beyond $\pm 3\,\sigma(t)$ are marked with blue lines. Transmitter off has been marked with green line.

noise). The $\hat{A}(t)$ and $\sigma(t)$ are determined from the minute values of the amplitudes (dB) of the 8 preceding quiet days (1–8 December). Since the period of the storm was geomagnetically quiet, perturbations beyond 1σ may also be associated with this TC, but for stronger confidence ($>$95%) we have considered the perturbations above 3σ for the analysis. The time is given in hours UT; local Fiji time is UT + 12:00. The plots show the normal diurnal variation with noise from scattering in the ionosphere. In general, the variability of the transmitter signals is high during the nighttime when the electron density decreases and the *D* region is more sensitive to magnetospheric conditions from the top and meteorological conditions from below, whereas in the daytime VLF wave propagation is quite stable, the daytime *D* region can be considered quite stable and dominated by the ionization by the solar Lyman α flux. The NPM and JJI signals are relatively stable, whereas the NLK and NAA signals have considerably larger variability, probably because of their longer propagation paths and the larger range of local time zones traveled. They may, therefore, be less

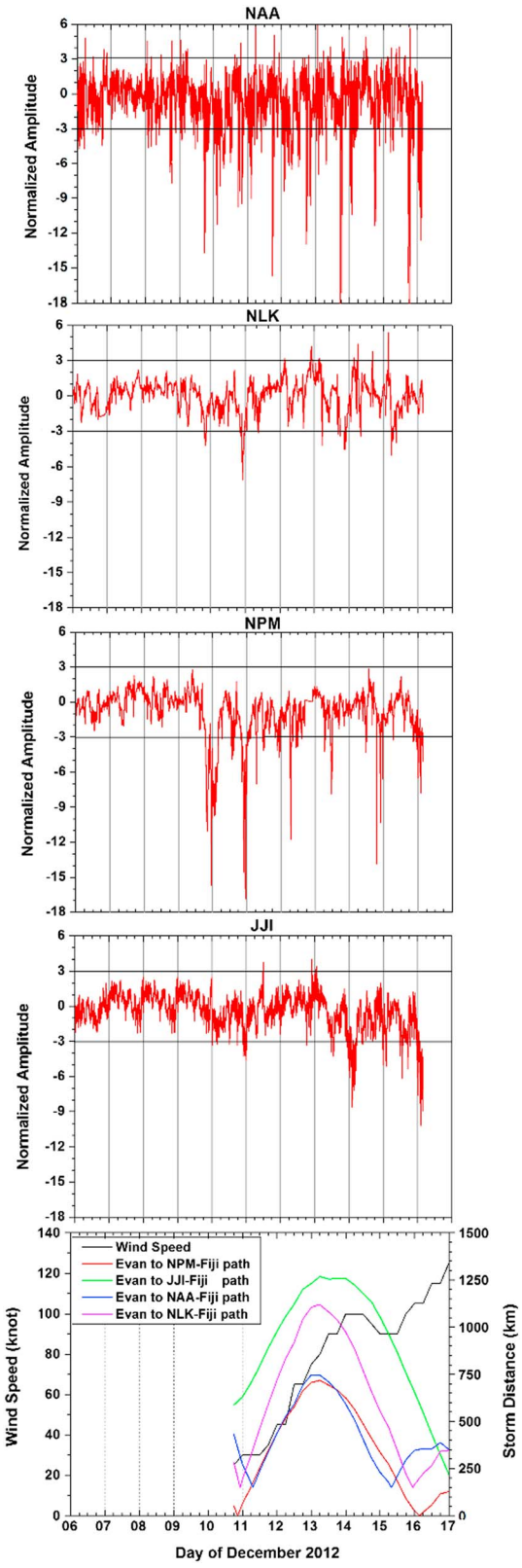

Figure 3. The normalized signal perturbations, $A_n(t)$ and the $\pm 3\sigma(t)$ levels (horizontal lines) for the four transmitter signals (first to fourth panels) during 6–16 December 2012. The distance from the storm center to the transmitter receiver great circle paths and the storm intensity (fifth panel).

sensitive to cyclone-induced perturbations. The periods of amplitude excursion beyond $\pm 3\ \sigma(t)$ are marked with blue horizontal lines. A period of NLK transmitter off is indicated with a green line. Amplitude anomalies are clearly seen, for instance, in the NPM signal amplitude which decreases below the -3σ level during the daytime on 10 December, during the night of 13 December and during the final hours before power was shut down in Fiji. On JJI signal, we also observed large negative anomalies above 3 $\sigma(t)$ on 14 December at 04 UT (not shown in Figure 2) and on 16 December at 03 UT (Figure 2, right column, bottom), reaching 4.2 dB and 5.7 dB, respectively. However, in some cases during the sunset and sunrise minima and at nighttime, the signal perturbations may not necessarily be associated with TC due to large day-to-day variability in depth of minima and sometimes in the nighttime signal.

The signal fluctuation during the complete period of analysis is shown in Figure 3. The plots begin on 6 December at 04:00 UT, 3 days before the formation of the storm. The 3 days are part of the 8 preceding quiet days used to establish the unperturbed baseline of the signals and are included to allow comparison of the quiet and perturbed periods. The parameter plotted is the normalized perturbation amplitude $A_n(t) = \left(A(t) - \hat{A}(t)\right)/\sigma(t)$. The horizontal lines on the graphs correspond to $A(t) = \hat{A}(t)$ and $A(t) = \hat{A}(t) \pm 3\sigma(t)$. On the fifth panel are shown the storm intensity and the distance of the storm center to the TRGCPs of the four transmitter links. It is clear from the plots that all transmitter signals are well within the 3σ level during the days prior the storm and have significant (relative to the 3σ level) anomalies during the storm, commencing around 00:00 UT on 10 December just prior to cyclone

classification when the storm was a tropical depression.

The anomalies (perturbations) are both positive and negative and occur both during day and night. Daytime perturbations to signal amplitudes are relatively rare because the ionosphere is robust with a high electron density which requires more powerful disturbances to affect VLF wave propagation. The fact that our data show disturbances during the daytime, points to a source like GWs that strongly perturb the whole atmosphere, shifting the altitude of the *D* region. In a few cases, the anomalies appear to be correlated in time, e.g., around 00:00 UT on 11 December and the last hours before receiver power shut down on 16 December. This supports the interpretation that the signals are perturbed by a common source in proximity to the receiver. The variation of storm center distance to the TRGCPs and the storm intensity in terms of wind speed during 6–17 December 2012 are shown in Figure 3 (fifth panel).We note that the transmitter links are affected even at maximum distance of the storm. The distance to the transmitter-receiver may play a role in the link of NPM where perturbations seem to decrease in magnitude at maximum distance and JJI where perturbations begin later in time.

3.2. Estimation of the Lower Ionospheric Changes

We have used LWPC code mentioned in the introduction to estimate the parameters H' and β (equation (1)) in an assumed TC-disturbed region. The model and the method have been used in the past for research into the *D* region of the ionosphere, establishing normal day and nighttime parameters that characterize the region [*McRae and Thomson*, 2000; *Thomson and McRae*, 2009], and for perturbed conditions for instance associated with solar eclipses [*Clilverd et al.*, 2001], solar flares [*Thomson et al.*, 2005], lightning-induced electron precipitation [*Poulsen et al.*, 1993a, 1993b], and geomagnetic storms [*Kumar et al.*, 2015]. However, this is the first time it is applied to perturbations related to convective storms of the troposphere.

We selected three clear events of VLF signal amplitude anomaly that surpassed 3σ for more than 2 h. The limit of 3σ has been taken in view of significant signal variability during sunset/sunrise and night of the paths. The first event is in the NPM signal during the nighttime on 13 December at 13:00 UT (14 December 01 LT) where the signal amplitude change (ΔA) relative to the unperturbed value was -3.0 dB and the phase change was +50° above 3σ phase relative to normal phase change during the event. To model this event the phase change was considered in addition to the amplitude change as NPM is a phase stable transmitter. The center of Evan was ~650 km from the transmitter link and ~1175 km from the receiver in Fiji. Using the LWPC V2.1 for 13 December at 13 UT, the ambient (along the path) values of H' and β given by the LWPC code are $\widehat{H'}$ = 87.0 km and $\hat{\beta}$ = 0.430 km^{-1}, respectively. As described earlier, these parameters are now assumed constant along the path except in the disturbed region of the TC where perturbations to the both H' and β are assumed to follow a Gaussian distribution out to 800 km from the peak in either direction along the path. Further details on the procedure could be found in paper by *NaitAmor et al.* [2016] where authors modeled early VLF perturbations events due to TLEs. The peak of the Gaussian perturbation was placed at 1250 km along the GCP from the receiver which was determined the by projection of TC center on the path. The disturbed values of H' and β at the maximum of the Gaussian that gives the best fit of the simulated signal parameters to measured ones are H'_d = 81.8 km (a decrease by 5.2 km) and β_d = 0.439 km^{-1} (an increase by 0.009 km^{-1}). The ionosphere parameters of the best fit are shown in Figure 4a. Finally, we determined from equation (1) the relative change in the electron density at the nighttime VLF reflection height of taken to be 90 km for the disturbed and undisturbed conditions, $N_e^d/\hat{N}_e$.The values of these parameters along with change in lower ionospheric parameters $\Delta H' = \left(\hat{H'} - H'_d\right)$ and $\Delta\beta = \left(\hat{\beta} - \beta_d\right)$ are shown in Table 2.

Two VLF events on the JJI signal have been analyzed where the signal anomalies were larger than 3σ for more than 3 h. They are both during the daytime. The geomagnetic conditions during TC Evan were quiet, and there were no solar flares of class C and above within 10 h of these events, so any contribution related with space weather conditions to these events is ruled out. Therefore, these induced VLF perturbation events are taken as locally associated with TC. However, effect of other factors such strong electric field between the clouds and the Earth, air-sea interaction etc. still remains unknown. It is also important to state here that the method used here cannot exactly find and examine the perturbed part of *D* region through which signal propagated and data obtained by other measuring technique can help us better solve such complex problem. The first event occurred on 14 December at 04:00 UT (not shown in Figure 2) when the storm

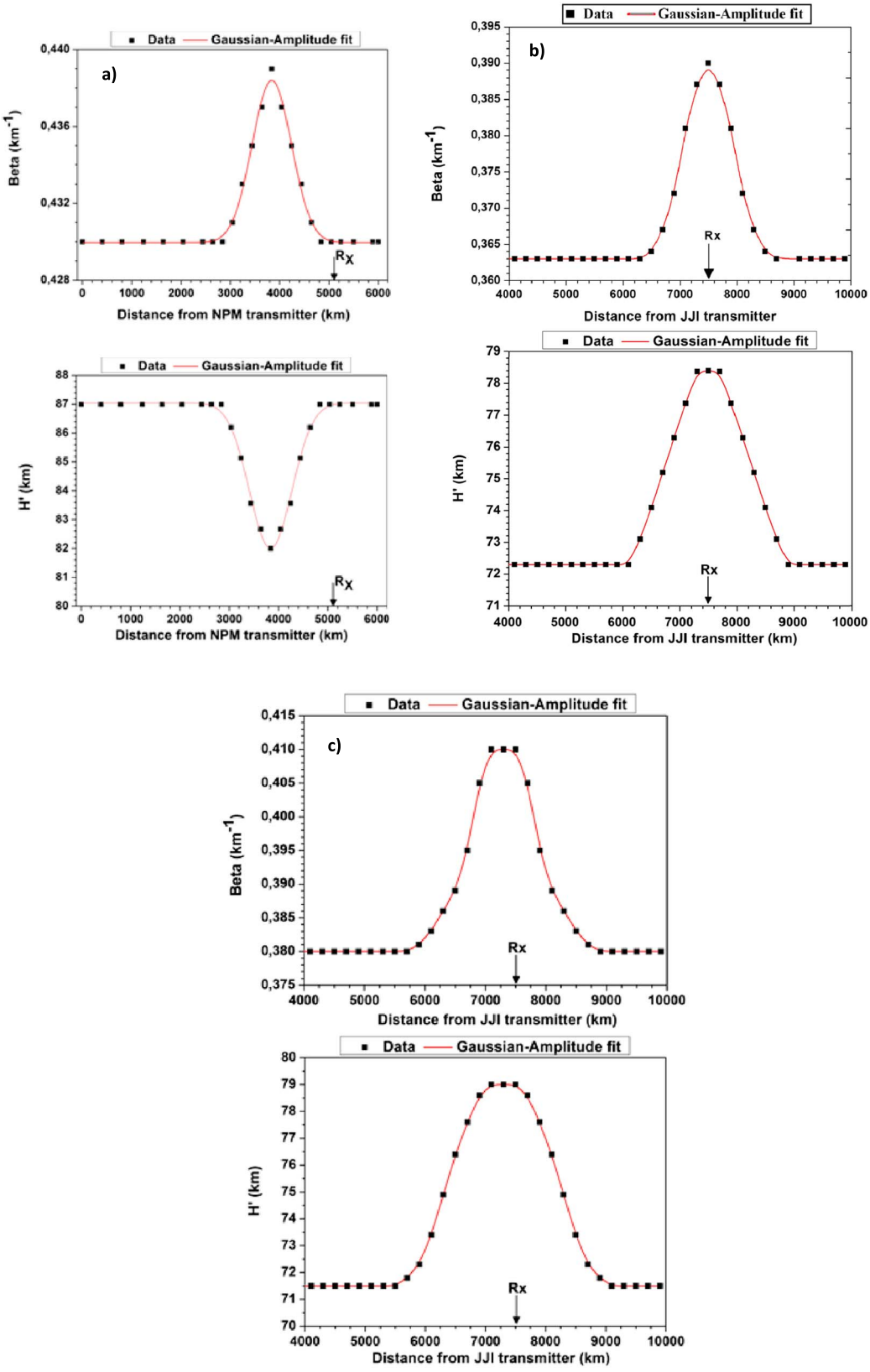

Figure 4. LWPC modeling of the following: (a) NPM signal anomaly on 13 December at 13 UT, (b) JJI signal anomaly on 14 December at 04 UT, (c) JJI signal anomaly on 16 December at 03 UT. The point (Rx) indicated by line with downward arrow represents the distance from transmitter where LWPC output has been taken and is within 30 km of the receiver location.

Table 2. *D* Region Parameters From LWPC Modeling for Three Anomaly Events

	ΔA (dB)	$\widehat{H'}$ (km)	H'_d (km)	$\Delta H'$ (km)	$\hat{\beta}$ (km^{-1})	β_d (km^{-1})	$\Delta\beta$ (km^{-1})	$N_e^d/\hat{N}_e$
NPM 13 Dec	−3.0	87.0	81.8	−5.2	0.430	0.439	+0.009	10/1
JJI 14 Dec	−4.2	72.3	78.4	+6.1	0.363	0.390	+0.027	1/10
JJI 16 Dec	−5.7	71.5	79.0	+7.5	0.380	0.410	+0.030	1/20

center was ~1200 km from the receiver, and the perturbation was 1.5 dB below 3σ. The second event occurred on 16 December at 03:00 UT when the TC center was ~400 km from the receiver and the perturbation was −3.0 dB below 3σ. The *D* region parameters, particularly during the daytime, are time dependent, even in the absence of any sudden ionospheric disturbances, due to variations in the ionizing radiation intensity which is dependent on the SZA and solar cycle. Since the VLF signal anomalies occurred during daytime, the SZA at midpath location (07.61°N, 156.00°E) of JJI-Suva on 14 December 2012 at 04 UT (the time of maximum signal decrease) has been used to find the ambient values of H' and β using the relationship given by *McRae and Thomson* [2000] that gives ambient value of $\widehat{H'}$ = 72.3 km and $\hat{\beta}$ = 0.363 km^{-1} for the unperturbed daytime ionosphere. The daytime ionosphere can be considered as horizontal uniform medium for significantly shorter path than JJI-Suva, and we take this approximation for the middle part of JJI-Suva path. We calculate the values of H' and β at the locations of transmitter and receiver at the time of maximum signal anomaly of events to show the limit of this validity. However, details study on it may be part of our future research. The values of H', β at the locations of transmitter (32.04°N, 130.81°E) and receiver (18.14°S, 178.44°E) for 14 December event are 73.4 km, 0.342 km^{-1}, and 73.2 km, 0.345 km^{-1}, respectively, and for 16 December event are 73.2 km, 0.345 km^{-1}, and 71.7 km, 0.373 km^{-1}, respectively. Thus, H' values at midpath location for both events are within 1.3–1.5% and 0.8–1.3% with respect to values at transmitter and receiver locations, respectively, whereas β values are approximately within 4–5%. *Nina and Čadež* [2014] for shorter daytime VLF (23.4 kHz) DHO transmitter (Rhauderfehn, Germany) path to Belgrade, Serbia, estimated percentage deviations in H' and β less than 1% which are less compared to our values due longer Suva-JJI propagation path. The amplitude perturbations above 3σ are modeled for a Gaussian disturbance centered over receiver for 14 December event and 400 km away from the receiver along the path for 16 December event to get perturbed values of H' and β at the maximum of the Gaussian disturbance. To model both these events, only amplitude perturbations were used as the JJI is not a phase stable transmitter. The ionosphere parameters of the best fit for 14 and 16 December events are shown in Figures 4b and 4c, respectively. The results along with change in lower ionospheric parameters $\Delta H' = \left(\widehat{H'} - H'_d\right)$ and $\Delta\beta = \left(\hat{\beta} - \beta_d\right)$ for both the events are given in Table 2. A significant change in the reference height($\Delta H'$) and electron density ($N_e^d/\hat{N}_e$) estimated using LWPC modeling from the ambient values corresponding to midpath location with not much appreciable change in sharpness factor ($\Delta\beta$) can be noted from Table 2. We note here that the Gaussian perturbation is introduced as a simple function to estimate the magnitude of the perturbations to the mesosphere that appear consistent with observations but is not meant as a model of GWs [*Mallen et al.*, 2005]. There could be, of course, a multitude of daytime *D* region disturbances that can give the observed perturbations.

We suggest that the changes in reference altitude are caused by lifting and sinking of the atmosphere due to upward GWs [*Marshall and Snively*, 2014] bringing the *D* region ionization with it, since the cyclone by itself does not modify source or loss mechanism of *D* region ionization. The change in electron density in Table 2 due to TC is calculated at the daytime VLF reflection height of 75 km and nighttime 90 km. *Vanina-Dart et al.* [2008] analyzed changes in the vertical profiles of the electron concentration during two TCs over the northern Indian Ocean using rocket sounding of the *D* region at Thumba rocket site (8°N, 77°E), India. They found a significant decrease (by a factor of 2–4) in the electron concentration at altitudes of 60–80 km and as a result increase in *D* region base height by several kilometers (not more than 5 km) over normal daytime values. *Lay and Shao* [2011] analyzing the time domain lightning waveforms at three Los Alamos Sferic Array stations associated with thunderstorms of 17 June 2005 have shown that nighttime *D* layer ionospheric height perturbations can be large by 6 km from average due to AGWs originating from this large convective thunderstorm activity overshooting the tropopause and perturbing the electron distribution in the *D* region. Our estimations for TC Evan show that the perturbations may be larger.

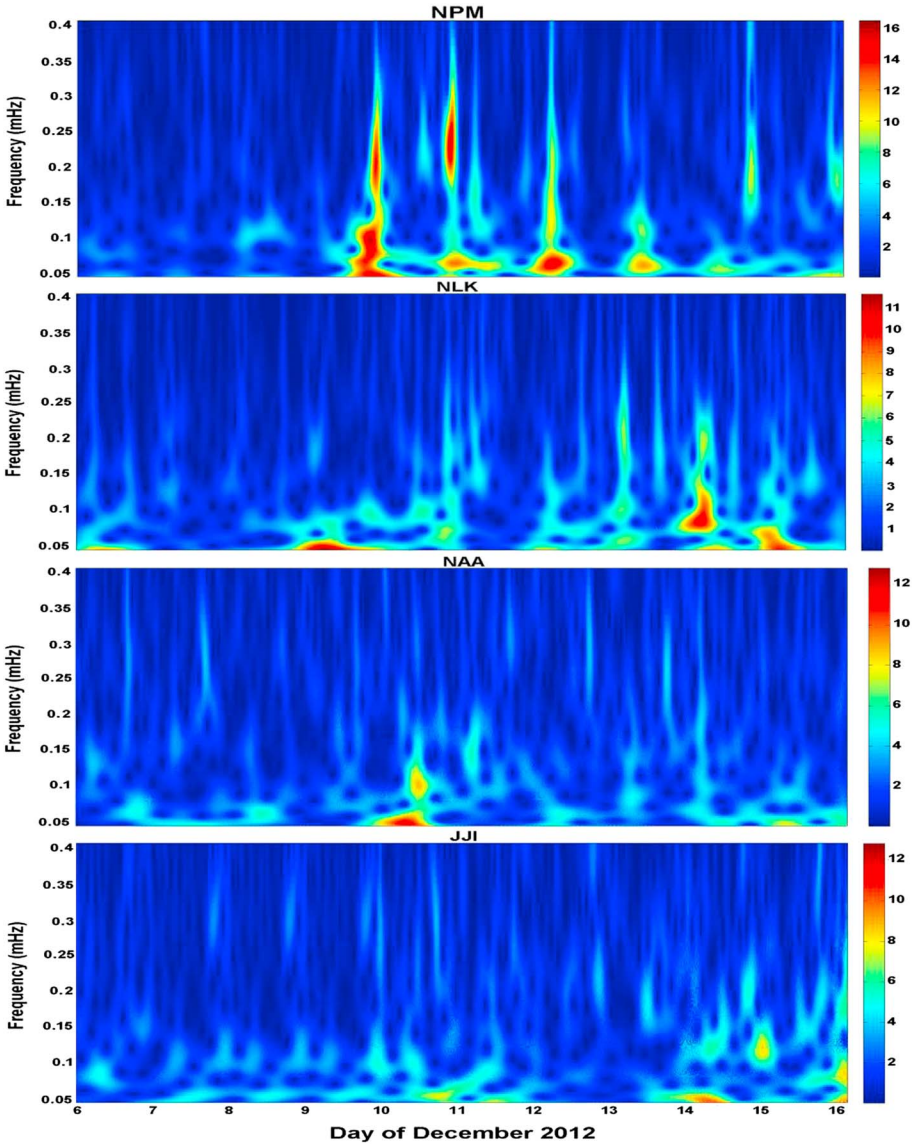

Figure 5. The Wavelet spectra based on the mother Morlet wavelet analysis of the four transmitter signals during 6–16 December 2012.

3.3. Wavelet Analysis of VLF Signals Amplitude: Wave-Like Signatures

The changes in the electron density and lower ionosphere may be caused by atmospheric GWs generated by the storm, as concluded in an analysis of ionospheric HF Doppler shift data from a station at Peking University during the passage of 24 typhoons (1987–1992) [*Xiao et al.*, 2007] and suggested by simulations [*Liu et al.*, 2014]. The analysis is applied to the perturbation amplitudes (not normalized by σ), $A_p(t) = A(t) - \hat{A}(t)$, where most of the diurnal variations are removed. It should be stated here that apart from waves generated by the solar terminator [*Nina and Čadež*, 2013], the signals are expected to be free from other common sources such as topographic effects because the TC was over the South Pacific Region with only a few minor islands in the region of the storm (e.g., Samoa). The Mother wavelet analysis of amplitude data showed that periods of detected wave-like signatures (WLS), in general, are in better agreement with periods of GWs obtained in other works than with periods of acoustic waves (AWs). The WLS having periods in the range 2–5 min are suggested due to AWs generated by the storms [*Xiao et al.*, 2007]. We applied a band-pass filter with lower frequency cutoff at 5×10^{-5} Hz (period of ~5 h and 33 min) to Mother Wavelet analysis to further reduce the influence of the terminator and with a high-frequency cutoff at 5×10^{-4} Hz (period of ~33 min) to

look at mainly the low-frequency GWs. The Wavelet spectra of filtered output of four transmitter signals are shown in Figure 5 as functions of time for the same time period as in Figure 3. We see the very clear transition from quiet days to TC disturbed days with WLS events associated with GWs starting on 9 December at frequencies 0.05–0.35 mHz corresponding to wave period from 45.7 min to 5.5 h. The NLK signal spectrum is most similar to the NPM signal spectrum, probably because their paths are the closest. The difference in the WLS amplitude may be caused by a larger NPM transmitter signal strength and larger day-to-day variability of NLK signal (smaller average). The WLS events are more frequent and clear as we move from the quiet to the disturbed period (9–16 December) and are seen most clearly in the NPM signal. The JJI transmitter shows little WLS activity until 13 December as could be expected because the storm is the farthest from this transmitter link and reaches it later than the others.

4. Discussion and Conclusions

We have analyzed perturbations of subionospheric VLF propagation and estimated the associated *D* region changes during the TC Evan which occurred in December 2012 in the South Pacific Region. A similar study of TC Dianmu in August 2010 based on transmitter signals received by three Russian stations in the eastern most part of Russia showed only negative nighttime anomalies during the 1–2 days when cyclone was inside the sensitivity zone of the subionospheric paths, with signals decreasing up to ~20 dB [*Rozhnoi et al.*, 2014]. Our results indicate that the amplitude anomalies can occur both in the day and nighttime. The negative and positive signal anomalies can be explained in terms of destructive and constructive interferences between the modes reflected from normal and disturbed segments of the waveguide. *Nina et al.* [2017] analyzed effects of 41 Tropical Depression (TD) events on NAA (in USA) VLF transmitter signal recorded at a station in Belgrade (Serbia) and found that 36 out of 41 TD events (88%) produced significant signal anomaly during daytime, nighttime, and sunset/sunrise periods.

If we relate the displacement of the *D* region altitude with the vertical wavelength and note that the wavelength of the diagnostic VLF transmitter signals is ~15 km we can summarize the characteristics of the WLS to a horizontal wavelength $>$ 15 km, a vertical wavelength $<$ 10 km, and the period from7 min to 5.5 h. The period is somewhat longer than the periods of 7–16 min and 15–55 min reported by *Rozhnoi et al.* [2014], analyzing VLF data for a TC during August 2010. In comparison, *Ming et al.* [2014] found that GWs closer to the source, in the upper troposphere and lower stratosphere using radiosonde and GPS radio occultation data, have vertical wavelengths in the range 0.7–3 km, horizontal wavelengths between 80 and 400 km, and periods of 4.6–13 h. *Dhaka et al.* [2003] analyzed GWs in the lower stratosphere using middle and upper atmosphere data from a MU radar during typhoon Orchid (9426) and found GWs in the period range of 7–8, 15, and 40–60 min. *Pfister et al.* [1993] reported GWs at ~110 km horizontal wavelength measured from aircraft over a typhoon. They further suggest that the scale is consistent with the scales of cell-like structures in the typhoon seen in the cloud top temperatures and that the waves can be generated by slow modulation in the altitude 400–600 m of the cells. *Vadas* [2007] suggested that the GWs with periods of 10–80 min and horizontal wavelengths of 100–1200 km can reach the ionosphere from their sources in the troposphere with weak background wind in middle atmosphere as a necessary condition for propagating upward [*Vadas et al.*, 2012; *Chou et al.*, 2017]. Although our results appear coherent with the past studies outlined above, a full simulation from the source to the mesosphere under different background wind is needed for proper comparison, which is out of scope for the present paper.

The *D* region may also be affected directly by the electromagnetic pulse from lightning discharges in the TC rain bands where the electric field may enhance the attachment rate of free electrons to neutral molecules, thereby reducing the conductivity of the lower edge of the ionosphere *D* region. A thunderstorm with a multitude of lightning may in this way change the reflection height of the illuminated region typically by 5 km [*Marshall et al.*, 2008] and that at nighttime the effect of TLE or lightning ionization is to increase the electron density at lower ionosphere. In addition, examining lightning rates from the World-Wide Lightning Location Network (http://webflash.ess.washington.edu/), we find that the rain bands do generate lightning but not at rates that approach those of thunderstorms. We conclude, therefore, that the most likely mechanism of lower ionospheric modification is via GWs as period of detected WLS events is in better agreement with periods of GWs reported in previous studies [e.g., *Dhaka et al.*, 2003; *Vanina-Dart and Sharkov*, 2016; *Song et al.*, 2017] than with periods of AWs. The GWs associated with mesoscale convective systems

(MCS) within TC become increasingly dominant with altitude having wide range of horizontal scales, from mesoscale to thousands of kilometers [*Lu et al*., 2014], supported by duration of signal perturbation that is more than 2 h for all three simulated VLF anomaly events in our study which is too long as compared to duration of early VLF perturbation events generated by single lighting or TLE.

We find that the perturbations began when the storm was a TD and before it was classified as a TC. We consider that perturbations were of local TC origin due to quite geomagnetic conditions during the TC. This begs the more general conclusion that large convective storms such as MCS that are above ~100 km in horizontal extent [e.g., *Lyons et al*., 2008], or thunderstorms that last for more than 6 h [e.g., *Lay et al*., 2015] likely influence the mesosphere through deposition of GW energy. This conclusion is coherent with simulations of wave generation by thunderstorms as in *Snively and Pasko* [2003] and with optical observations of thunderstorm-generated GWs in the upper mesosphere (modulations of airglow) presented in *Yue and Lyons* [2015].

We finally note that perturbations are strong and coherent between transmitter signals when the storm is close to the signal paths to the receiver, as early in the storm phase and a period before power cut, and that perturbations were observed out to ~1200 km distance from the transmitter links in agreement with the conclusions of *Waldock and Jones* [1987] that at midlatitude the ionospheric disturbances produced by GWs can occur within 1500 km horizontally to tropical storms.

Acknowledgments
Authors are thankful to European Science Foundation Network TEA-IS (Thunderstorm Effects and the Atmosphere-Ionosphere System) for providing visiting scholarship to Sushil Kumar and Samir NaitAmor at National Space Institute, Technical University of Denmark (DTU Space), Denmark, during January 2016 when a significant part of data analysis and planning of the paper was carried out. Author (S.K.) is thankful to The University of the South Pacific for providing financial support under Strategic Research Theme for carrying out this work. The VLF data recorded during the TC are available with corresponding author.

References

Araki, T. (1973), Anomalous diurnal changes of trans-equatorial VLF radio waves, *J. Atmos. Terr. Phys.*, *35*, 693–703, doi:10.1016/0021-9169(73)90200-6.

Beharrell, M., J. F. Honary, C. J. Rodger, and M. A. Clilverd (2015), Substorm induced energetic electron precipitation: Morphology and prediction, *J. Geophys. Res. Space Physics*, *120*, 2993–3008, doi:10.1002/2014JA020632.

Barr, R., D. L. Jones, and C. J. Rodger (2000), ELF and VLF radio waves, *J. Atmos. Sol. Terr. Phys.*, *62*, 1689–1718.

Clilverd, M. A., C. J. Rodger, N. R. Thomson, J. Lichtenberger, P. Steinbach, P. Cannon and M. J. Angling (2001), Total solar eclipse effects on VLF signals: Observation and modeling, *Radio Sci.*, *36*(4), 773–788, doi:10.1029/2000RS002395.

Chou, M. Y., C. C. H. Lin, J. Yue, H. F. Tsai, Y. Y. Sun, J. Y. Liu, and C. H. Chen (2017), Concentric traveling ionosphere disturbances triggered by super typhoon Meranti (2016), *Geophys. Res. Lett.*, *44*, 1219–1226, doi:10.1002/2016GL072205.

Cowling, D. H., H. D. Webb, and C. K. Yeh (1971), Group rays of internal gravity waves in a wind-stratified atmosphere, *J. Geophys. Res.*, *76*, 200–213, doi:10.1029/JA076i001p00213.

Dhaka, S. K., I. M. Takahash, Y. Shibagaki, M. D. Yamanaka, and S. Fukao (2003), Gravity wave generation in the lower stratosphere due to passage of the typhoon 9426 (Orchid) observed by the MU radar at Shigaraki (34.85°N, 136.10°E), *J. Geophys. Res.*, *108*(D19), 4595, doi:10.1029/2003JD003489.

Ferguson, J. A. (1998), Computer programs for assessment of long-wavelength radio communications, version 2.0: User's guide and source files, *No. TD-3030*, Space and Naval Warfare Syst. Cent., San Diego, Calif.

Ferguson, J. A., and F. P. Snyder (1987), The segmented waveguide program for long wave-length propagation calculation, Tech. Doc1071, Naval Ocean System Center, San Diego, 285, Calif.

Fritts, D. C., and M. J. Alexander (2003), Gravity wave dynamics and effects in the middle atmosphere, *Rev. Geophys.*, *41*(1), 1003, doi:10.1029/2001RG000106.

Garcia, R. R., and S. Solomon (1985), The effect of breaking gravity waves on the dynamics and chemical composition of the mesosphere and lower thermosphere (1985), *J. Geophys. Res.*, *90*, 3850–3868, doi:10.1029/JD090iD02p03850.

Haldoupis, C., M. Cohen, B. Cotts, E. Arnone, and U. Inan (2012), Long-lasting *D*-region ionospheric modifications caused by intense lightning in association with elve and sprite pairs, *J. Geophys. Res.*, *39*, L16801, doi:10.1029/2012GL052765.

Kikuchi, T. (1983), Anomalous diurnal phase shifts of omega VLF waves (10–14 kHz) on the east–west low latitude and transequatorial paths, *J. Atmos. Terr. Phys.*, *45*(11), 743–751.

Kumar, P., and E. F. Georgiou (1997), Wavelet analysis for geophysical applications, *Rev. Geophys.*, *35*, 385–412, doi:10.1029/97RG00427.

Kumar, S., A. Kumar, F. Menk, A. K. Maurya, R. Singh, and B. Veenadhari (2015), Response of the low-latitude D region ionosphere to extreme space weather event of 14–16 December 2006, *J. Geophys. Res. Space Physics*, *120*, 788–799, doi:10.1002/2014JA020751.

Lay, E. H., and X.-M. Shao (2011), Multi-station probing of thunderstorm-generated *D*-layer fluctuations by using time-domain lightning waveforms, *Geophys. Res. Lett.*, *38*, L23806, doi:10.1029/2011GL049790.

Lay, E. H., X.-M. Shao, A. K. Kendrick, and C. S. Carrano (2015), Ionospheric acoustic and gravity waves associated with midlatitude thunderstorms, *J. Geophys. Res. Space Physics*, *120*, 6010–6020, doi:10.1002/2015JA021334.

Liu, H.-L., J. M. McInerney, S. Santos, P. H. Lauritzen, M. A. Taylor, and N. M. Pedatella (2014), Gravity waves simulated by high-resolution whole atmosphere community climate model, *Geophys. Res. Lett.*, *41*, 9106–9112, doi:10.1002/2014GL062468.

Lyons, W. A., S. A. Cummer, M. A. Stanley, G. R. Huffines, K.C. Wiens, and T. E. Nelson (2008), Supercells and sprites, *Bull. Am. Meteorol. Soc.*, *89*, 1165–1174, doi:10.1175/2008BAMS2439.1.

Lynn, K. J. W. (1967), Anomalous sunrise effects observed on a long transequatorial VLF propagation path, *Radio Sci.*, *2*(6), 521–530, doi:10.1002/rds196726521.

Mallat, S. (1998), *A Wavelet Tour of Signal Processing*, pp. 102–115, Academic Press, San Diego, Calif.

Mallen, K. J., M. T. Montgomery, and B. Wang (2005), Reexamining the near-core radial structure of the tropical cyclone primary circulation: Implications for vortex resiliency, *J. Atmos. Sci.*, *62*, 408–425, doi:10.1175/JAS-3377.1

Marshall, R. A., U. S. Inan, and T. W. Chevalier (2008), Early VLF perturbations caused by lightning EMP-driven dissociative attachment, *Geophys. Res. Lett.*, *35*, L21807, doi:10.1029/2008GL035358.

Marshall, R. A., and J. B. Snively (2014), Very low frequency subionospheric remote sensing of thunderstorm-driven acoustic waves in the lower ionosphere, *J. Geophys. Res. Atmos.*, *119*, 5037–5045, doi:10.1002/2014JD0215940.

Ming, F. C., C. Ibrahim, C. Barthe, S. Jolivet, P. Keckhut, Y.-A. Liou, and Y. Kuleshov (2014), Observation and a numerical study of gravity waves during tropical cyclone Ivan (2008), *Atmos. Chem. Phys.*, *14*, 641–658, doi:10.5194/acp-14-641-2014.

McRae, W. M., and N. R. Thomson (2000), VLF phase and amplitude: Daytime ionospheric parameters, *J. Atmos. Sol. Terr. Phys.*, *62*, 609–618.

NaitAmor, S., H. Ghalila, and M. B. Cohen (2016), TLEs and early VLF events: Simulating the important impact of transmitter-disturbance-receiver geometry, *J. Geophys. Res. Space Physics*, *121*, 792–801, doi:10.1002/2016JA022791.

Nina, A., and V. M. Čadež (2013), Detection of acoustic-gravity waves in lower ionosphere by VLF radio waves, *Geophys. Res. Lett.*, *40*, 4803–4807, doi:10.1002/grl.50931.

Nina, A., and V. M. Čadež (2014), Electron production by solar Ly-alpha line radiation in the ionospheric *D*-region, *Adv. Space Res.*, *54*, 1276–1284, doi:10.1016/j.asr.2013.12.042.

Nina, A., M. Radovanović, B. Milovanović, A. Kovačević, J. Bajčetić, and L. Č. Popović (2017), Low ionospheric reactions on tropical depressions prior hurricanes, *Adv. Space Res.*, doi:10.1016/j.asr.2017.05.024, in press.

Perevalova, N. P., and A. B. Ishin (2011), Effects of tropical cyclones in the ionosphere from data of sounding by GPS signals, *Atmos. Oceanic Phys.*, *47*, 1072–1083, doi:10.1134/S000143381109012X.

Peter, W. B., and U. S. Inan (2005), Electron precipitation events driven by lightning in hurricanes, *J. Geophys. Res.*, *110*, A05305, doi:10.1029/2004JA010899.

Pfister, L., K. R. Chan, T. P. Bui, S. Bowen, M. Legg, B. Gary, K. Kelly, M. Proffitt, and W. Starr (1993), Gravity waves generated by a tropical cyclone during the STEP tropical field program: A case study, *J. Geophys. Res.*, *98*, 8611–8638, doi:10.1029/92JD01679.

Poulsen, W. L., U. S. Inan, and T. F. Bell (1993a), A multiple-mode three-dimensional model of VLF propagation in the Earth-ionosphere waveguide in the presence of localized *D* region disturbances, *J. Geophys. Res.*, *98*, 1705–1717, doi:10.1029/92JA01529.

Poulsen, W. L., T. F. Bell, and U. S. Inan (1993b), The scattering of VLF waves by localized ionospheric disturbances produced by lightning induced electron precipitation, *J. Geophys. Res.*, *98*, A9, 15,553–15,559, doi:10.1029/92JA01529.

Rozhnoi, A., M. Solovieva, B. Levin, M. Hayakawa, and V. Fedun (2014), Meteorological effects in the lower ionosphere as based on VLF/LF signal observations, *Nat. Hazards Earth Syst. Sci.*, *14*, 2671–2679, doi:10.5194/nhessd-2-2789-2014.

Song, Q., F. Ding, X. Zhang, and T. Mao (2017), GPS detection of the ionospheric disturbances over China due to impacts of typhoons Rammasum and Matmo, *J. Geophys. Res. Space Physics*, *122*, 1055–1063, doi:10.1002/2016JA023449.

Sato, K., S. Watanabe, Y. Kawatani, Y. Tomikawa, K. Miyazaki, and M. Takahashi (2009), On the origins of mesospheric gravity waves, *Geophys. Res. Lett.*, *36*, L19801, doi:10.1029/2009GL039908.

Sauli, P., P. Abry, P. Boska, and L. Duchayne (2006), Wavelet characterization of ionospheric acoustic and gravity waves occurring during solar eclipse of August 11, 1999, *J. Atmos. Sol. Terr. Phys.*, *68*, 586–598, doi:10.1016/j.jastp.2005.03.024.

Silber, I., and C. Price (2016), On the use of VLF narrowband measurements to study the lower ionosphere and the mesosphere–lower thermosphere, *Surv. Geophys.*, *34*, 255–292, doi:10.1007/s10712-013-9222-6.

Snively, J. B., and V. P. Pasko (2003), Breaking of thunderstorm-generated gravity waves as a source of short-period ducted waves at mesopause altitudes, *Geophys. Res. Lett.*, *30*(24), 2254, doi:10.1029/2003GL018436.

Thomson, N. R., and W. M. McRae (2009) Nighttime ionospheric *D* region: Equatorial and nonequatorial, *J. Geophys. Res.*, *114*, A08305, doi:10.1029/2008JA014001.

Thomson, N. R., C. J. Rodger, and M. A. Clilverd (2005), Large solar flares and their ionospheric *D*-region enhancements, *J. Geophys. Res.*, *110*, A06306, doi:10.1029/2005JA011008.

Thomson, N. R., M. A. Clilverd, and C. J. Rodger (2014), Low-latitude ionospheric D region dependence on solar zenith angle, *J. Geophys. Res. Space Physics*, *119*, 6865–6875, doi:10.1002/2014JA020299.

Vanina-Dart, L. B., and E. A. Sharkov (2016), Main results of recent investigations into the physical mechanisms of the interaction of tropical cyclones and the ionosphere, *Atmos. Oceanic Phys.*, *52* (9), 1120–1127, doi:10.1134/S0001433816090279.

Vanina-Dart, L. B., I. V. Pokrovskaya, and E. A. Sharkov (2008), Response of the lower equatorial ionosphere to strong tropospheric disturbances, *Geomagn. Aeron.*, *48*, 245–250, doi:10.1134/S001679320802014X.

Vadas, S. L. (2007), Horizontal and vertical propagation and dissipation of gravity waves in the thermosphere from lower atmospheric and thermospheric sources, *J. Geophys. Res.*, *112*, A06305, doi:10.1029/2006JA011845.

Vadas, S., J. Yue, and T. Nakamura (2012), Mesospheric concentric gravity waves generated by multiple convective storms over the North American great plain, *J. Geophys. Res.*, *117*, D07113, doi:10.1029/2011JD017025.

Wait, J. R., and K. P. Spies (1964), Characteristics of the Earth-ionosphere waveguide for VLF radio waves, *Tech. Note 300*, Natl. Bur. of Stand., Boulder, Colo.

Waldock, J. A., and T. B. Jones (1987), Source regions of medium scale travelling ionospheric disturbances observed at mid-latitudes, *J. Atmos. Terr. Phys.*, *9*, 2, 105, doi:10.1016/0021-9169(87)90044-4.

World Meteorological Organization (2013), A case study of tropical cyclone Evan around Samoa. [Available at www.pacificdisaster.net/dox/pdn_nd_20111217_1223.pdf.]

Xiao, Z., S. Xiao, Y. Hao, and D. Zhang (2007), Morphological features of ionospheric response to typhoon, *J. Geophys. Res.*, *112*, A04304, doi:10.1029/2006JA011671.

Yue, J., and W. A. Lyons (2015), Structured elves: Modulation by convectively generated gravity waves, *Geophys. Res. Lett.*, *42*, 1004–1011, doi:10.1002/2014GL062612.